

A NEUTRON STAR STIFF EQUATION OF STATE DERIVED FROM COOLING PHASES OF THE X-RAY BURSTER 4U 1724–307

VALERY SULEIMANOV^{1,2}, JURI POUTANEN³, MIKHAIL REVNIVTSEV⁴, AND KLAUS WERNER¹

¹ Institute for Astronomy and Astrophysics, Kepler Center for Astro and Particle Physics, Eberhard Karls University, Sand 1, 72076 Tübingen, Germany; suleimanov@astro.uni-tuebingen.de, werner@astro.uni-tuebingen.de

² Kazan Federal University, Kremlevskaja Str., 18, Kazan 420008, Russia

³ Astronomy Division, Department of Physics, P.O. Box 3000, FI-90014 University of Oulu, Finland; juri.poutanen@oulu.fi

⁴ Space Research Institute (IKI), Russian Academy of Sciences, Profsoyuznaya 84/32, Moscow 117997, Russia

Received 2011 February 11; accepted 2011 September 5; published 2011 November 15

ABSTRACT

Thermal emission during X-ray bursts is a powerful tool for determining neutron star (NS) masses and radii if the Eddington flux and the apparent radius in the cooling tail can be measured accurately and distances to the sources are known. We propose here an improved method of determining the basic stellar parameters using the data from the cooling phase of photospheric radius expansion (PRE) bursts covering a large range of luminosities. Because at that phase the blackbody apparent radius depends only on the spectral hardening factor (color correction), we suggest fitting the theoretical dependences of the color correction versus flux in Eddington units to the observed variations of the inverse square root of the apparent blackbody radius with the flux. For that we use a large set of atmosphere models for burst luminosities varying by three orders of magnitude and for various chemical compositions and surface gravities. We show that spectral variations observed during a long PRE burst from 4U 1724–307 are entirely consistent with the theoretical expectations for the passively cooling NS atmospheres. Our method allows us to more reliably determine both the Eddington flux (which is found to be smaller than the touchdown flux by 15%) and the ratio of the stellar apparent radius to the distance. We then find a lower limit on the NS radius of 14 km for masses below $2.3 M_{\odot}$, independently of the chemical composition. These results suggest that the matter inside NSs is characterized by a stiff equation of state. We also find evidence in favor of hydrogen-rich accreting matter and obtain an upper limit to the distance of 7 kpc. We finally show that the apparent blackbody emitting area in the cooling tails of the short bursts from 4U 1724–307 is two times smaller than that for the long burst and their evolution does not follow the theory. This makes their usage for determining the NS parameters questionable and casts serious doubt on the results of previous works that used similar bursts from other sources for analysis.

Key words: radiative transfer – stars: neutron – X-rays: bursts – X-rays: individual (4U 1724–307) – X-rays: stars

Online-only material: color figures

1. INTRODUCTION

Studies of the thermal emission from neutron stars (NSs) have been used extensively to determine their masses and radii (e.g., Damen et al. 1990; van Paradijs et al. 1990; Lewin et al. 1993; Rutledge et al. 2002; Heinke et al. 2006; Webb & Barret 2007; Özel et al. 2009; Güver et al. 2010a), which can provide constraints on the properties of the matter at supranuclear densities (Haensel et al. 2007; Lattimer & Prakash 2007). Thermonuclear X-ray bursts at NS surfaces and, particularly, the photospheric radius expansion (PRE) bursts exceeding the Eddington limit at high-flux phases (Kuulkers et al. 2003) are excellent laboratories for such detailed studies. The observed Eddington flux gives a constraint on the NS mass–radius relation. This method, however, suffers from the uncertainty in determining the exact moment when the luminosity reaches the Eddington limit at the NS surface, which is often assumed to coincide with the moment of “touchdown,” when the measured color temperature is highest and the apparent radius is smallest (Damen et al. 1990). This interpretation is uncertain because the touchdown flux typically coincides with the maximum flux (Galloway et al. 2008b), while the latter is expected to be larger than the surface Eddington flux by the redshift factor $1+z$ (Lewin et al. 1993).

The second constraint can be obtained from the apparent radius of the NS at late stages of the burst. This method also has systematic uncertainties related to the color-correction

factor $f_c = T_c/T_{\text{eff}}$ (the ratio of the color temperature to the effective temperature of the star), which is a function of the burst luminosity.

To minimize the theoretical uncertainties in modeling the burst atmospheres at nearly Eddington luminosities, we proposed (Suleimanov et al. 2011) to use the whole cooling track and check that the evolution of the blackbody normalization with flux is consistent with the theoretically predicted evolution for a passively cooling NS.

The unique determination of mass and radius requires one more constraint. Knowing the distance to a burster breaks the degeneracy; therefore, bursters located in globular clusters would be of interest. For the analysis in the present paper we choose 4U 1724–307, which resides in the globular cluster Terzan 2. We analyze three PRE bursts from that source and show that they follow different cooling tracks. We also speculate on the reasons for such a discrepancy. We demonstrate that the apparent blackbody radius for the long PRE burst evolves according to the predictions for the passively cooling NS with a constant apparent surface, and we use these data to determine the NS parameters.

2. DATA

2.1. X-Ray Bursts from 4U 1724–307

For our analysis we have used the data from the Proportional Counter Array (PCA) spectrometer of the *Rossi X-ray Timing*

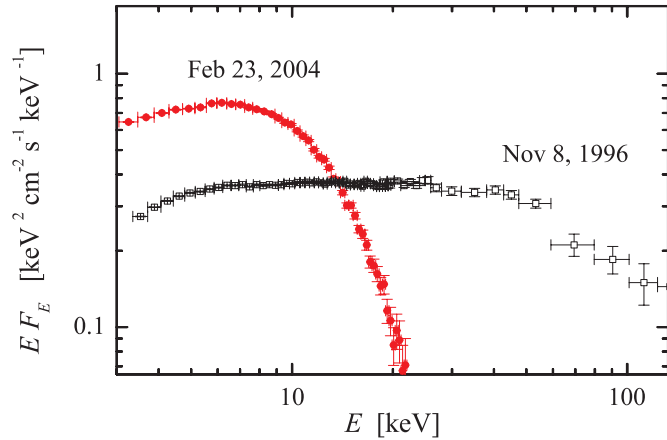


Figure 1. Spectra of the persistent emission before the long burst (open squares) and one of the short bursts (filled circles).

(A color version of this figure is available in the online journal.)

Explorer (*RXTE*) because they provide us with the maximum possible number of photons within the small time intervals, during which the spectrum of the X-ray burst varies very little. The *RXTE*/PCA data were analyzed using the HEASOFT package (version 6.6.1). Response matrices were generated using the task PCARSP (version 10.1) of this package. The background of the PCA detectors was estimated using the CM_bright_VLE model. In order to account for the uncertainties reflecting the quality of the *RXTE*/PCA response matrix, a 1% systematic error (Jahoda et al. 2006) was added in quadrature to the statistical error in each PCA energy channel. The spectral fitting was performed using the XSPEC (version 11) package (Arnaud 1996).

RXTE observed three PRE bursts from 4U 1724–307 (Galloway et al. 2008a). A long (>150 s) PRE burst was recorded on 1996 November 8 (Molkov et al. 2000). Two short PRE bursts were observed on 2004 February 23 and May 22. The quiescent emission around these three bursts was significantly different. The long burst happened when the source was in the so-called hard/low state with a luminosity of a few percent of the Eddington luminosity and the X-ray emission was formed in an optically thin medium. The short bursts were observed during the high/soft state, with the X-ray emission characterized by the optically thick accretion disk and the boundary/spreading layer from the NS surface. The spectra of the persistent emission of 4U 1724–307 are presented in Figure 1. All burst spectra were fitted assuming an absorption column density of $N_H = 10^{22} \text{ cm}^{-2}$, corresponding to the best-fit value for the persistent spectrum. But fitting using N_H as a free parameter was also performed.

X-ray bursts often have thermally looking spectra that can be approximated by a blackbody (Galloway et al. 2008a). However, the fits of the burst spectra with an absorbed blackbody model give a rather high $\chi^2/\text{dof} \sim 2\text{--}3$. This is not very surprising because the photon number is large, with the errors being dominated by the systematics. Theoretical models of the NS atmosphere during X-ray bursts do not predict exact blackbody spectral shapes, but the residuals in the 3–20 keV *RXTE* energy band are expected at the level of 4%–5% (see Figure 8 in Suleimanov et al. 2011). The residuals between the blackbody model and the data of X-ray bursts of 4U 1724–307 have similar amplitudes (see Figures 2 and 3). Adopting the systematic uncertainty of the model at the level of 3%–5% allows us

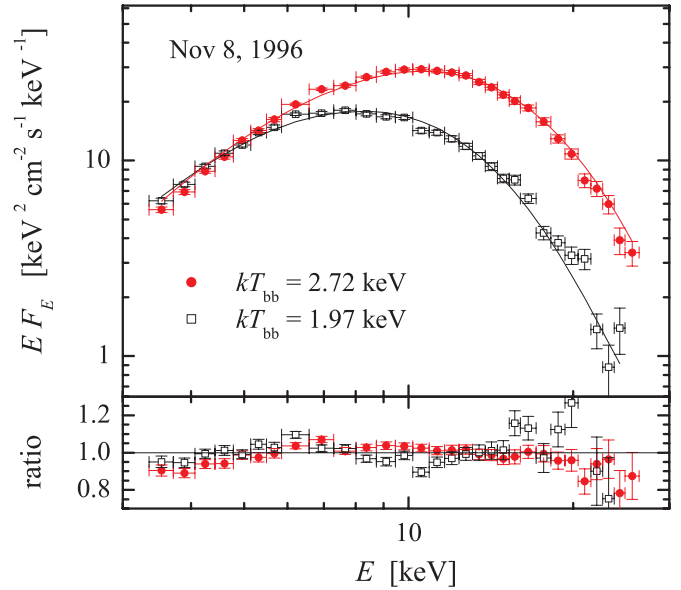


Figure 2. Evolution of the long burst spectra at early decline burst phases with the corresponding best-fit blackbody models (solid curves). The corresponding time points are shown by arrows in the middle panel of Figure 4.

(A color version of this figure is available in the online journal.)

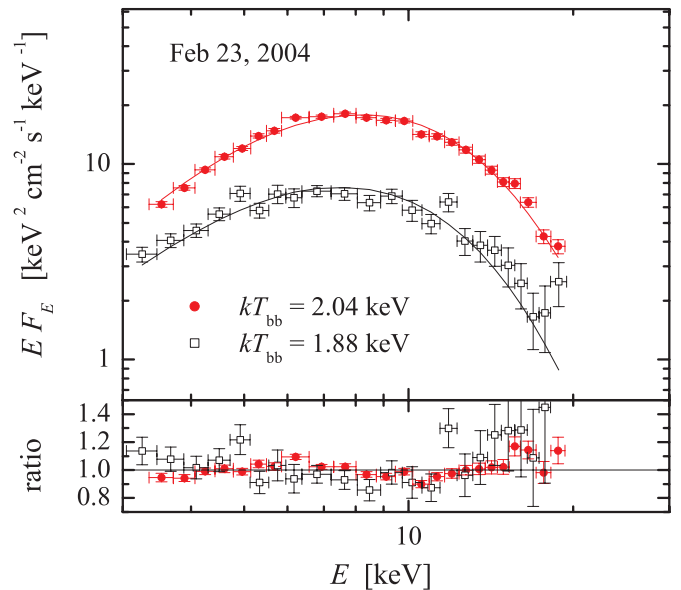


Figure 3. Same as Figure 2, except for a short burst.

(A color version of this figure is available in the online journal.)

to obtain acceptable χ^2 values for all spectra at the cooling tails of the analyzed X-ray bursts, while a simple blackbody analytical model allows us to correctly represent the general shape of the spectrum in the 3–20 keV energy band. Therefore, in our subsequent analysis we use simple blackbody models for approximating the spectral shapes and compare the obtained parameters with those obtained by fitting the spectra produced by the full theoretical NS atmosphere model in the same energy band.

The best-fit parameters of the employed blackbody model are the color temperature T_{bb} and the normalization constant $K \equiv (R_{bb}[\text{km}]/D_{10})^2$ (the blackbody radius is measured in kilometers and the distance D to the source in units of 10 kpc). These can be combined to estimate the observed bolometric flux F .

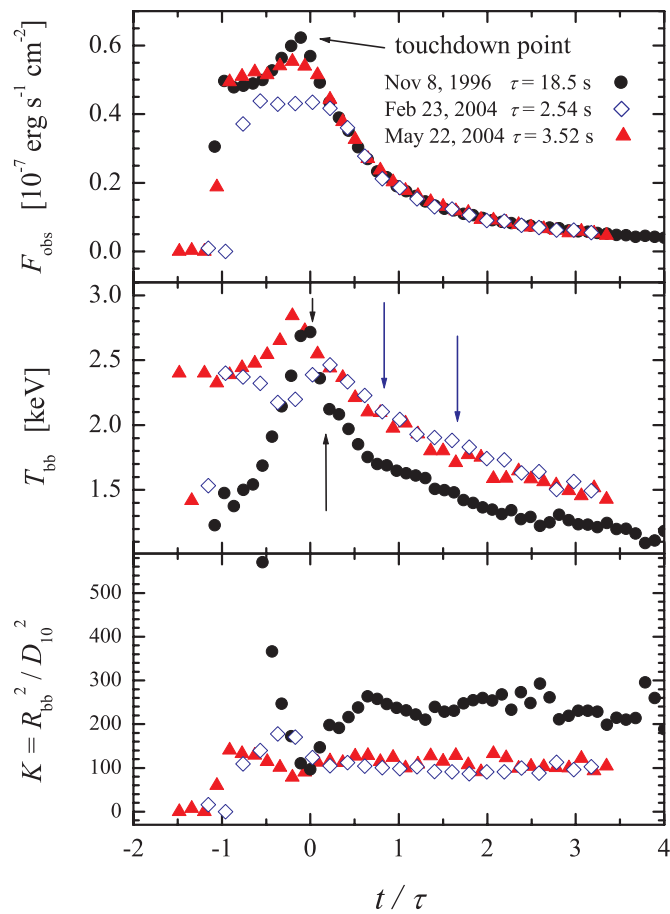


Figure 4. Evolution of the observed blackbody fluxes, color temperatures, and normalizations $K = R_{\text{bb}}^2 / D_{10}^2$ for three bursts from 4U 1724–307 in 1996 November 8 (black circles), 2004 February 23 (blue diamonds), and 2004 May 22 (red triangles). The time variable is normalized to the characteristic decay time τ , which is equal to 18.5, 2.54, and 3.52 s for these three bursts, respectively. For the long burst, the zero time corresponds to the touchdown point (marked by an arrow in the upper and middle panels), while the light curves were shifted for the short burst so that the cooling tails coincide. The arrows show the times when the spectra shown in Figures 2 and 3 were collected.

(A color version of this figure is available in the online journal.)

The evolution of the fitted parameters during the bursts is shown in Figure 4. The time is normalized to the individual flux decay timescales τ and shifted to allow an easy comparison between the bursts. The time point, when the flux and the color temperature T_{bb} reach their maximum values and the normalization K has a minimum, is usually named the “touchdown” point (shown by the arrow in the upper and middle panels of Figure 4 for the long burst). The maximal fluxes of the short bursts are appreciably smaller than that for the long burst. Their normalizations do not show a significant rise at the early stages of the bursts, indicating that the NS photosphere has not substantially expanded.

The most serious difference between the short and long bursts is the normalization value at the flux decay phase, which is approximately two times larger in the long burst (Figure 5). The natural explanation for that is the presence of the optically thick accretion disk, which, in the soft state, blocks a significant part of the NS apparent surface, while the hot, optically thin, transparent accretion flow in the hard state does not affect the NS apparent area much. In addition to that effect, there could be additional differences in the physical conditions of the NS atmosphere (and thus in spectral hardening factors), as the boundary/spreading

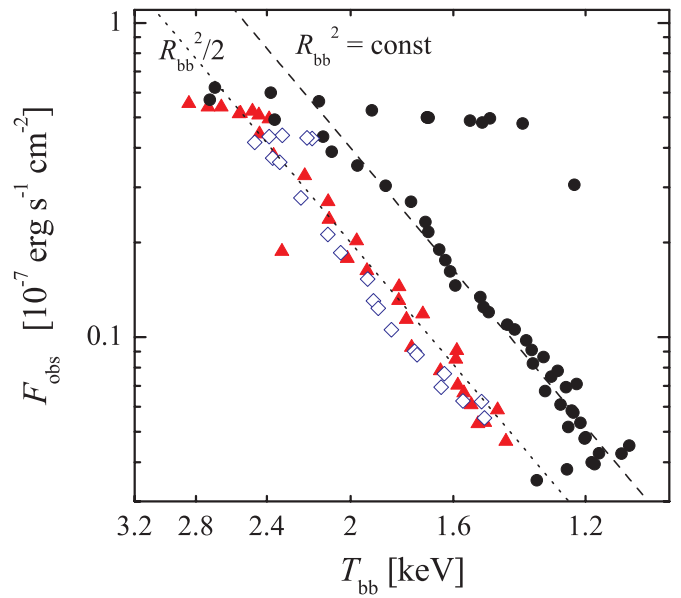


Figure 5. Evolution of the bursts in the flux–temperature plane for the three bursts from Figure 4. The curves of constant R_{bb}^2 describing the decay phase are also shown. The blackbody apparent area for the short bursts (dotted curve) is a factor of two smaller than the corresponding area describing the long burst (dashed curve).

(A color version of this figure is available in the online journal.)

layer in the soft state forces the NS atmosphere to rotate close to Keplerian velocity (Inogamov & Sunyaev 1999; Suleimanov & Poutanen 2006). We note that similar differences between short and long bursts were also found in another X-ray bursting NS (Galloway et al. 2008a; Zhang et al. 2010).

2.2. Distance to 4U 1724–307

4U 1724–307 resides in the globular cluster Terzan 2. The distance to that $D = 7.5 \pm 0.7$ kpc was measured by Kuchinski et al. (1995), while Ortolani et al. (1997) give $D = 5.3 \pm 0.6$ kpc, if $R_V = A_V / (B - V) = 3.6$ (more suitable for red stars; see Grebel & Roberts 1995), or 7.7 ± 0.6 kpc if $R_V = 3.1$. To cover all possibilities, we further assume a flat distribution from 5.3 to 7.7 kpc with Gaussian tails of $1\sigma = 0.6$ kpc on both ends.

3. METHOD

3.1. Basic Relations

Here we briefly present some well-known relations between observed and real physical NS parameters, which arise due to the gravitational redshift and the light bending. The observed luminosity L_∞ , effective temperature T_∞ , and apparent NS radius R_∞ are connected with the luminosity at the NS surface L , the effective temperature measured at the surface T_{eff} , and the NS circumferential radius R and mass M by the following relations (Lewin et al. 1993):

$$L_\infty = \frac{L}{(1+z)^2}, \quad T_\infty = \frac{T_{\text{eff}}}{1+z}, \quad R_\infty = R(1+z), \quad (1)$$

with the redshift factor

$$1+z = (1 - 2GM/Rc^2)^{-1/2}. \quad (2)$$

The gravity g on the NS surface is larger in comparison with the Newtonian case due to the general relativity effects

$$g = \frac{GM}{R^2}(1+z); \quad (3)$$

therefore, the Eddington luminosity is larger, too:

$$L_{\text{Edd}} = \frac{4\pi GMc}{\kappa_e}(1+z) = 4\pi R^2 \sigma_{\text{SB}} T_{\text{Edd}}^4. \quad (4)$$

Here T_{Edd} is the maximum possible effective temperature on the NS surface, $\kappa_e = 0.2(1+X) \text{ cm}^2 \text{ g}^{-1}$ is the electron (Thomson) scattering opacity, and X is the hydrogen mass fraction. The observed Eddington luminosity is smaller for higher z :

$$L_{\text{Edd},\infty} = \frac{4\pi GMc}{\kappa_e} \frac{1}{1+z}. \quad (5)$$

This is related to the observed Eddington flux

$$F_{\text{Edd}} = \frac{L_{\text{Edd},\infty}}{4\pi D^2} = \frac{GMc}{\kappa_e D^2} \frac{1}{1+z} \quad (6)$$

and the Eddington temperature

$$T_{\text{Edd},\infty} = \left(\frac{gc}{\sigma_{\text{SB}} \kappa_e} \right)^{1/4} \frac{1}{1+z} = \left(\frac{F_{\text{Edd}}}{\sigma_{\text{SB}}} \right)^{1/4} \left(\frac{R_\infty}{D} \right)^{-1/2}, \quad (7)$$

which is the effective temperature corresponding to the Eddington flux at the NS surface corrected for the gravitational redshift. We note here that the electron scattering opacity decreases with temperature (e.g., Paczynski 1983; Pozdniakov et al. 1983), and is reduced by about 7% at the temperature of $\sim 3 \text{ keV}$, which is typical for the upper layers of the luminous NS atmospheres. This affects the luminosity where the Eddington limit actually is reached.

3.2. Atmosphere Models and Color Correction

Numerous computations of X-ray bursting NS atmospheres (London et al. 1984, 1986; Ebisuzaki 1987; Madej 1991; Pavlov et al. 1991; Zavlin et al. 1996; Suleimanov & Poutanen 2006; Suleimanov et al. 2011) show that their emergent spectra at high luminosities are close to diluted blackbody spectra due to strong energy exchange between high-energy photons and relatively cold electrons at NS surface layers (Compton down-scattering),

$$F_E \approx w B_E(T_c = f_c T_{\text{eff}}), \quad (8)$$

where f_c is the color-correction (or hardness) factor and w is the dilution factor, which at high luminosities is very close to $1/f_c^4$ (Suleimanov et al. 2011).

Spectra observed from the X-ray bursting NSs are close to thermal, and usually they are fitted by a blackbody with two parameters: the observed color temperature T_{bb} and the normalization $K = (R_{\text{bb}}(\text{km})/D_{10})^2$. It is easy to find the relations between various temperatures:

$$T_{\text{bb}} = f_c T_\infty = f_c \frac{T_{\text{eff}}}{1+z} = \frac{T_c}{1+z}. \quad (9)$$

The observed blackbody flux is then

$$F = \sigma_{\text{SB}} T_{\text{bb}}^4 \frac{R_{\text{bb}}^2}{D^2} = \sigma_{\text{SB}} T_\infty^4 \frac{R_\infty^2}{D^2} \quad (10)$$

and we can find the relation between the normalization and the NS radius:

$$\frac{R_{\text{bb}}^2}{D^2} = \frac{R^2}{D^2} \frac{(1+z)^2}{f_c^4} = \frac{R_\infty^2}{D^2} \frac{1}{f_c^4}. \quad (11)$$

These formulae can be transformed into the relation between color correction and normalization (Penninx et al. 1989; van Paradijs et al. 1990):

$$K^{-1/4} = f_c A, \quad A = (R_\infty[\text{km}]/D_{10})^{-1/2}. \quad (12)$$

A combination of A and F_{Edd} gives the Eddington temperature,

$$T_{\text{Edd},\infty} = 1.14 \times 10^8 A F_{\text{Edd},-7}^{1/4} \text{ K} = 9.81 A F_{\text{Edd},-7}^{1/4} \text{ keV}, \quad (13)$$

where $F_{\text{Edd},-7} = F_{\text{Edd}}/10^{-7} \text{ erg cm}^{-2} \text{ s}^{-1}$.

A detailed comparison of the theoretical models with the data requires the knowledge of the run of the color correction with flux. Previous models covered the range of luminosities very sparsely. Using our recently developed code (Suleimanov & Poutanen 2006; Suleimanov et al. 2006; Suleimanov & Werner 2007), we have computed a very detailed set of models with the luminosity varying by three orders of magnitude (Suleimanov et al. 2011).

An atmosphere model is fully defined by the surface gravity g , chemical composition, and the ratio of the luminosity to the Eddington luminosity $l = L/L_{\text{Edd}}$. The last parameter also relates the effective temperature to the Eddington temperature at the NS surface:

$$T_{\text{eff}} = l^{1/4} T_{\text{Edd}}. \quad (14)$$

We considered various chemical compositions (pure hydrogen, pure helium, and a solar mixture of hydrogen and helium with various metal abundances) and three surface gravities $\log g = 14, 14.3$, and 14.6 . The (redshifted) radiation spectrum from the NS atmosphere was then fitted with a diluted Planck function in the 3–20 keV energy band (i.e., the range observed by *RXTE*) to determine the color-correction factor f_c (see Figure 6). The behavior of f_c at relatively high l depends mainly on the hydrogen abundance X and very little on the surface gravity and metal abundance.

3.3. Determining M and R Using the Touchdown Method

In an ideal situation if the observed X-ray emission indeed comes from the passively cooling, fully visible NS and the distance to the source is known, we can determine NS mass M and radius R from two observables: the Eddington flux given by Equation (6) and the NS apparent blackbody size in the cooling tail, or quantity $A = K^{-1/4}/f_c$ (see, e.g., Lewin et al. 1993). The latter is related to the apparent size of the NS through the color correction, $R_\infty = f_c^2 R_{\text{bb}}$, and f_c is assumed to be known in the burst tail from the theoretical considerations. Although this method was proposed a long time ago, only recently have strong claims appeared in the literature suggesting that it can actually be used for determining accurate parameters of three bursting NSs (Özel et al. 2009; Güver et al. 2010a, 2010b).

Using the approach advertised in the aforementioned papers, one has to determine the Eddington flux from observations. For PRE bursts it was assumed that it is reached at the “touchdown” point (Damen et al. 1990), when the color temperature is highest and the apparent blackbody area is lowest. The color-correction factor f_c at the late cooling phases of the PRE bursts was taken to be close to 1.4 (Özel et al. 2009; Güver et al. 2010a, 2010b) based on the models by Madej et al. (2004) and Majczyna et al.

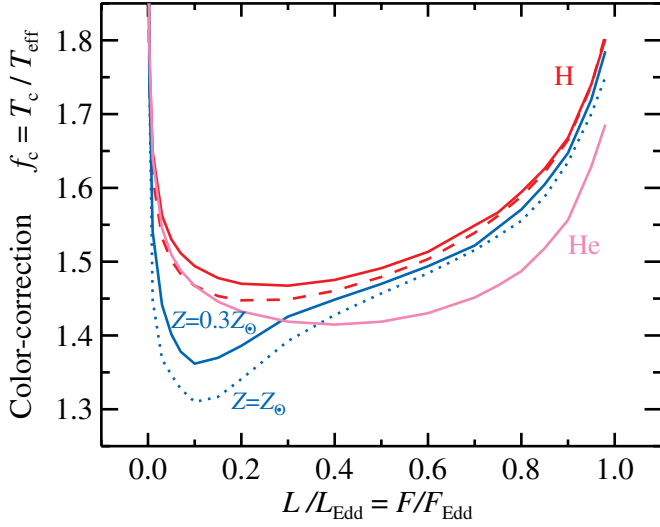


Figure 6. Color-correction factor as a function of the NS luminosity (Suleimanov et al. 2011). The curves correspond to atmospheres of different chemical compositions: pure hydrogen (red), pure helium (pink); the blue curves are for models with solar H/He composition plus solar abundance of metals $Z = Z_\odot$ (dotted blue) and subsolar metals $Z = 0.3 Z_\odot$ (solid blue). The surface gravity is taken to be $g = 10^{14.0} \text{ cm s}^{-2}$. The dashed curve shows the results for a hydrogen atmosphere at a larger gravity of $\log g = 14.3$.

(A color version of this figure is available in the online journal.)

(2005; see the discussion below). The observables can then be transferred to the constraints on M and R (see Figure 7). We will further call this approach the “touchdown method.”

From the Eddington flux estimate we have (see dotted curves in Figure 7)

$$R = \frac{2\kappa_e D^2 F_{\text{Edd}}}{c^3} u^{-1} (1-u)^{-1/2} = 14.138 \text{ km} (1+X) D_{10}^2 F_{\text{Edd},-7} u^{-1} (1-u)^{-1/2} \quad (15)$$

and the mass is found using

$$\frac{M}{M_\odot} = \frac{R}{2.95 \text{ km}} u, \quad (16)$$

where the compactness $u = R_S/R = 1 - (1+z)^{-2}$ and $R_S = 2GM/c^2$ is the Schwarzschild radius of the NS. A measurement of A gives another constraint:

$$R = R_\infty \sqrt{1-u} = f_c^2 D \sqrt{K} = D_{10} A^{-2} \sqrt{1-u} \text{ km}. \quad (17)$$

Combining this with the parametric expression (Equation (16)) for the mass, we get the second relation between M and R shown by the dashed curves in Figure 7.

The Eddington temperature given by Equation (13) is independent of the uncertain distance to the source and can be used to express the NS radius through the observables and u :

$$R = \frac{c^3}{2\kappa_e \sigma_{\text{SB}} T_{\text{Edd},\infty}^4} u (1-u)^{3/2}, \quad (18)$$

and the mass is then found via Equation (16). The corresponding relation between M and R is shown by the solid curve in Figure 7.

All three curves cross in one or two points (see Figure 7) if the quadratic equation

$$u(1-u) = \frac{2\kappa_e D F_{\text{Edd}}}{\sqrt{K} f_c^2 c^3} = 14.138 (1+X) D_{10} F_{\text{Edd},-7} A^2, \quad (19)$$

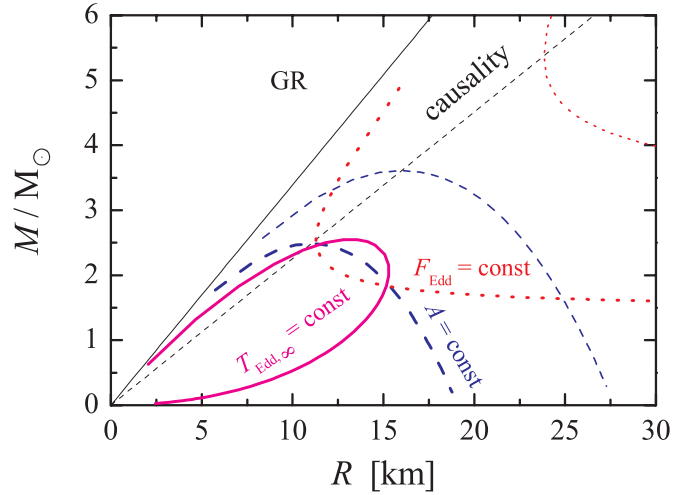


Figure 7. Constraints on M and R from various observed values. The solid curve gives the relation obtained from the Eddington temperature given by Equation (13); the thick dotted curve is for the Eddington flux given by Equation (6); the thick dashed curve is for $A = \text{const}$. If the assumed distance is too large, there are no solutions (the corresponding curves for $F_{\text{Edd}} = \text{const}$ and $A = \text{const}$ shown by thin lines do not cross).

(A color version of this figure is available in the online journal.)

which follows from Equations (15) and (17), has a real solution for u (see, e.g., Steiner et al. 2010). This happens if $u(1-u) < 1/4$ and the distance then should satisfy the following inequality:

$$D \leq D_{\text{max}} = \frac{\sqrt{K} f_c^2 c^3}{8 F_{\text{Edd}} \kappa_e} = \frac{0.177}{(1+X) A^2 F_{\text{Edd},-7}} \text{ kpc}. \quad (20)$$

In the opposite case, there is no physical solution for M and R for the given observables.

As we mentioned above, this method of determination for M and R works in an ideal situation. There are a few problems with this approach. First, the relation of the Eddington flux to the touchdown flux is not clear. The reduction of the electron scattering opacity at high temperatures increases the true Eddington limit by about 7% above that given by Equations (5) and (6). Also, if we believe that the X-ray burst luminosity is equal to the Eddington luminosity during the expansion phase of the PRE burst, the observed luminosity has to decrease when the photospheric radius decreases according to Equation (5) (Lewin et al. 1993). In reality, the observed luminosity in 4U 1724–307 increases when the photospheric radius decreases (see Figure 4). This implies that the ratio of the luminosity to the Eddington limit at the photosphere has to increase with decreasing photospheric radius (i.e., increasing redshift z). A combination of this dependence with the gravitational redshift effect then predicts that the observed luminosity reaches the maximum when the photospheric radius is larger than R , and that the maximum is larger than expected for the Eddington luminosity at the surface.

Second, the assumption of $f_c \approx 1.4$ in the cooling tail is very uncertain. This assumption is based on X-ray burst atmosphere models from Majczyna et al. (2005), who claimed a rather constant f_c at low effective temperatures (see also Figure 6 in Güver et al. 2010a), as well as the fact that most of the short PRE bursts have a constant normalization at late phases. We note here that the factors f_c in Majczyna et al. (2005) correspond to the ratio of the energy where the peak of the model flux F_E is reached to the peak energy of the blackbody spectrum at an effective temperature. Moreover, the low-luminosity models were calculated for high surface

gravity instead of low effective temperatures, which leads to incorrect results (see Suleimanov et al. 2011 for details). The color corrections obtained in this way, however, should not be compared with the data at all because the color temperatures of the time-resolved spectra from X-ray bursts are computed by *fitting* the actual data in a specific energy interval (e.g., 3–20 keV for *RXTE*/PCA) with the diluted blackbody function with arbitrary normalization. On the other hand, the values of f_c shown in Figure 6 are produced using the procedure similar to that applied to the data, i.e., by fitting the model spectra in the 3–20 keV range. As was shown by Suleimanov et al. (2011) the color correction has a flat part at $l \sim 0.2$ – 0.5 for most of the chemical compositions, but the actual value of f_c depends on the hydrogen fraction, e.g., for $X = 1$ it is closer to 1.5 than to 1.4 (see Figure 6). At lower luminosities f_c can first drop because of iron edges and then increase to rather high values. Thus, there is no unique value for f_c in the cooling tail. The expected significant variations of f_c with flux also imply that constancy of the apparent blackbody area in the cooling tail contradicts the burst atmosphere models. Therefore, the bursts showing such behavior obviously demonstrate influence of some physics not included in these simplest models of NS atmospheres, and thus cannot be used for the determination of NS masses and radii with the help of the aforementioned models.

Third, different PRE bursts from the same source show different cooling tracks, e.g., the long burst and the short bursts of 4U 1724–307 (see Figure 4) have normalizations different by a factor of two. This makes the determination of the apparent area from a single burst non-unique.

And finally, the most serious problem with this approach is that only *two* numbers from the information obtained from the cooling tail of the burst are used, and these quantities are not checked to determine whether they are actually consistent with each other. For example, the theory also predicts that the color correction f_c changes from ≈ 1.7 to ≈ 1.4 when the luminosity drops from the Eddington to about one-third of the peak value. This also implies that the blackbody normalization between the touchdown point and the decay phase must increase at least by a factor of two. It is really true for the long burst from 4U 1724–307, while the short bursts have nearly constant K , which is two times smaller than that in the long burst, implying probably a partial eclipse of the NS by the optically thick accretion disk and/or the influence of the boundary layer on the structure of the NS atmosphere (as discussed in Section 2.1). We also note here that all bursts analyzed by Özel et al. (2009) and Güver et al. (2010a, 2010b) are short, they do not show enough variations of K in their cooling tracks, and, therefore, the results obtained from these bursts are not reliable (see Section 5.2 for more details).

On the basis of all of these arguments, we offer a new approach to the NS mass and radius estimations using the information from the whole cooling track.

3.4. Determining M and R Using the Cooling Tail Method

If the radiating surface area does not change during the burst decay phase, the evolution of the normalization is fully determined by the color-correction variations (see Equations (11) and (12)). We thus suggest fitting the observed relation $K^{-1/4}-F$ at the cooling phase of the burst by the theoretical relations f_c-L/L_{Edd} (shown in Figure 6; see also Suleimanov et al. 2011), with free parameters being A and the Eddington flux F_{Edd} (see Figure 8 for illustration). The behavior of f_c depends rather weakly on the NS gravity and chemical composition, which

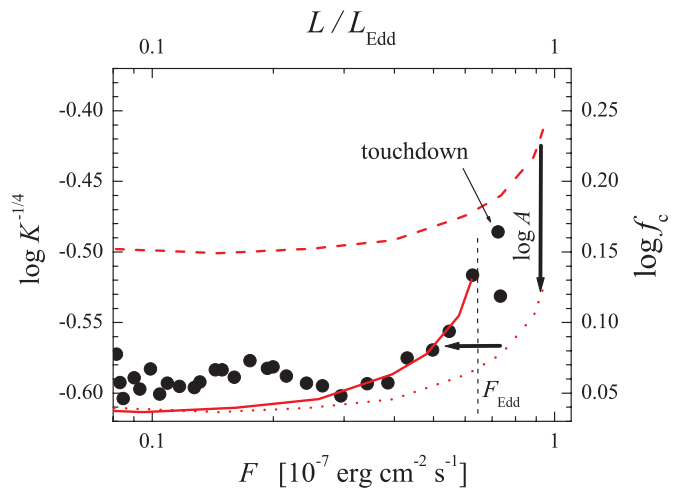


Figure 8. Illustration of the suggested new cooling tail method. The dependence $K^{-1/4}-F$ is shown as observed during the cooling track of the long burst from 4U 1724–307 on 1996 November 8 (circles). The theoretical f_c-L/L_{Edd} dependence is shown by the dashed curve (right and upper axes) and the best-fit relation (solid curve).

(A color version of this figure is available in the online journal.)

substantially reduces the model dependence of the fitting procedure. Using the obtained best-fit parameters, we can then apply a method identical to that described in Section 3.3.

The main advantages of the proposed cooling tail method are that there is no freedom in choosing f_c in the cooling tail; the determination of the Eddington flux becomes decoupled from the uncertainties related to the touchdown flux because the whole cooling tail is used; and finally, one can immediately check whether the burst spectral evolution is consistent with theoretical models and whether the employed model includes the majority of the relevant physics for the description of the considered phenomenon. This check can help choose for further analysis only those bursts that follow the theory.

4. RESULTS

4.1. The Long Burst from 4U 1724–307

4.1.1. Determining NS Parameters Using the Cooling Tail Method

Let us apply the method described in Section 3.4 for determining the NS mass and radius from the data on the long burst from 4U 1724–307. We fit the dependence of the normalization constant K on the observed flux F for the long burst by the theoretical curves f_c-L/L_{Edd} computed for three chemical compositions. They give a good description of the data at intermediate fluxes to the right of the dashed vertical line, but below the touchdown (Figure 9), and we use those data points for fitting. Close to the touchdown, significant deviations are probably caused by deviations from the plane-parallel atmosphere and the effects of the wind (thus, the models are not reliable). Strong deviations are also visible at low fluxes where the burst spectrum is probably modified by accretion. Assuming that F_{Edd} is actually reached at the touchdown contradicts the following evolution of the parameters during the cooling phase. The fits are better for the hydrogen-rich atmospheres. The results of the fitting for all of the considered chemical compositions of the NS atmosphere are presented in Table 1. The uncertainties in A and F_{Edd} are obtained with a bootstrap method.

Using the distance within the range of 5.3–7.7 kpc (see Section 2.2), we convert a distribution of F_{Edd} and A using Monte

Table 1
Best-fit Parameters

Atmosphere Model	F_{Edd} ($10^{-7} \text{ erg s}^{-1} \text{ cm}^{-2}$)	A ($\text{km}/10 \text{ kpc})^{-1/2}$	$T_{\text{Edd},\infty}$ (10^7 K)	χ^2/dof	M (M_{\odot})	R (km)
Hydrogen	0.525 ± 0.025	0.170 ± 0.001	1.64 ± 0.02	5.0/5	$1.9 \pm 0.4/2.45 \pm 0.15$ 1.4 (fixed)	$14.7 \pm 0.8/11.7 \pm 1.3$ 14.2 ± 0.4
Solar H/He, $Z = 0.3 Z_{\odot}$	0.521 ± 0.020	0.172 ± 0.002	1.66 ± 0.02	5.8/5	$1.85 \pm 0.6/2.7 \pm 0.15$ 1.4 (fixed)	$15.5 \pm 1.5/13.0 \pm 1.0$ 15.2 ± 0.4
Helium	0.50 ± 0.02	0.178 ± 0.002	1.71 ± 0.02	11.3/5	$1.05^{+0.55}_{-0.4}$ 1.4 (fixed)	$18.0^{+3.5}_{-3.5}$ 20.2 ± 0.5

Notes. Results of the fits to the $K^{-1/4}$ – F dependence with the NS atmosphere models for various chemical compositions and $\log g = 14.0$. For hydrogen and solar composition atmospheres there are two solutions for M and R (see Figure 10). Neutron star mass and radius are computed from A and F_{Edd} assuming a flat distribution of the distance between 5.3 and 7.7 kpc with Gaussian tails of $1\sigma = 0.6$ kpc. Errors correspond to the 90% confidence level.

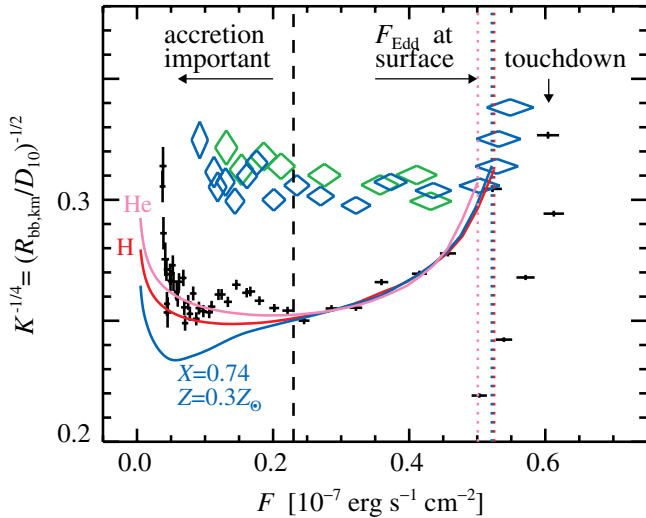


Figure 9. Comparison of the X-ray burst data for 4U 1724–307 to the theoretical models of the NS atmosphere. The crosses present the observed dependence of $K^{-1/4}$ vs. F for the long burst, while the diamonds represent two short bursts for the blackbody model with constant absorption $N_{\text{H}} = 10^{22} \text{ cm}^{-2}$. The solid curves correspond to the three best-fit theoretical models for the various chemical compositions (see Figure 6). The best-fit parameters F_{Edd} and A , defined by Equations (6) and (12), are given in Table 1.

(A color version of this figure is available in the online journal.)

Carlo simulations to the distribution of M and R (Figure 10 and Table 1). Because of the uncertainty in the distance, the resulting contours are elongated along the curves of the constant Eddington temperature. The pure helium model atmospheres give a mass that is too small from the stellar evolution point of view. It is also below the mass-shedding limit if the star is rotating faster than about 500 Hz. Pure hydrogen atmosphere models are consistent with the data only for $D < 6$ kpc, while the upper limit on the distance is 7 kpc for the atmosphere of the solar composition. The hydrogen-rich atmosphere models give a lower limit on the stellar radius of 14 km independently of the metal abundance (see Table 1) for NS masses less than $2.3 M_{\odot}$, and smaller radii are allowed only for high NS masses. For the helium atmosphere, the solution shifts toward higher masses and larger radii exceeding the mass-shedding limit (e.g., for a 1.5 solar mass star the radius is about 20 km). If we take the canonical NS mass of $1.4 M_{\odot}$, the NS radius is then strongly constrained at $R = 15.2 \pm 0.4 \text{ km}$ assuming solar H/He composition with $Z = 0.3 Z_{\odot}$ and $14.2 \pm 0.4 \text{ km}$ for hydrogen. The obtained constraints (see Table 1) imply a stiff equation of state of the NS matter.

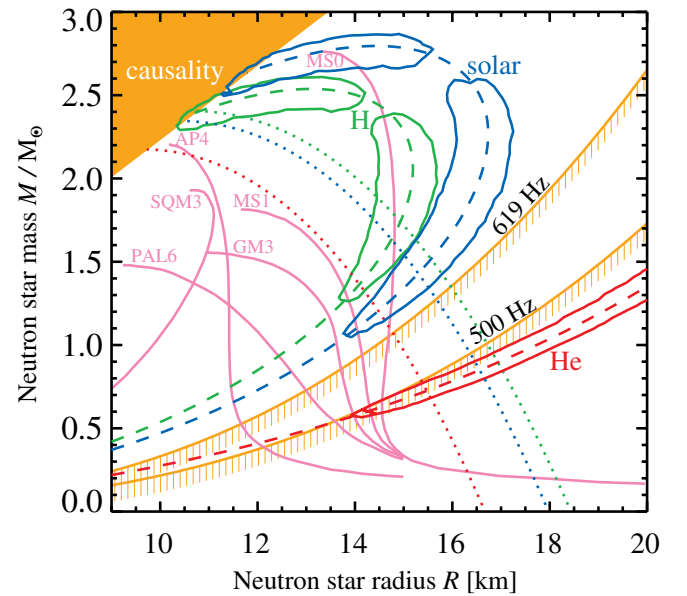


Figure 10. Constraints on the mass and radius of the NS in 4U 1724–307 from the long burst spectra (fitted with the blackbody model and constant absorption). The dotted curves correspond to the best-fit parameter A for the distance to the source of 5.3 kpc. For a flat distribution of the distance between 5.3 and 7.7 kpc with Gaussian tails of $1\sigma = 0.6$ kpc, the constraints are shown by contours (90% confidence level). They are elongated along the (dashed) curves corresponding to the Eddington temperatures $T_{\text{Edd},\infty}$ given by Equation (13) (which do not depend on the distance). These correspond to the three chemical compositions: green for pure hydrogen, blue for the solar ratio of H/He and subsolar metal abundance $Z = 0.3 Z_{\odot}$ appropriate for Terzan 2 (Ortolani et al. 1997), and red for pure helium. The mass–radius relations for several equations of state of the neutron and strange star matter are shown by solid pink curves. The upper left region is excluded by constraints from the causality requirements (Haensel et al. 2007; Lattimer & Prakash 2007). The brown solid curves in the lower right region correspond to the mass-shedding limit and delineate the zone forbidden for 4U 1724–307, if it had a rotational frequency of 500 or 619 Hz, which is the highest detected for the X-ray bursters (Strohmayer & Bildsten 2006).

(A color version of this figure is available in the online journal.)

The choice of the highest flux point at the $K^{-1/4}$ – F plot used in the fitting procedure affects the results slightly. Neglecting even the second point after the touchdown reduces the estimated F_{Edd} by 3%, while A (defined by the horizontal part of the cooling track) remains unchanged. This leads to a 2% increase in radius and a 4% decrease in the NS mass estimates. The fits to the $K^{-1/4}$ – F dependence, which is obtained with blackbody fits with free N_{H} in the same flux intervals as for constant N_{H} , give values of A about 10% smaller, while the Eddington flux estimates remain the same within 1%. In this case, the

estimated NS radii grow by 20% relative to those shown in Figure 10.

In addition, there is a systematic uncertainty of about 10% in the absolute values of fluxes measured by the *RXTE* (Kirsch et al. 2005; Weisskopf et al. 2010). It acts similarly to an additional 5% uncertainty on the distance and does not affect the value of $T_{\text{Edd},\infty}$. With the current uncertainty on the distance to 4U 1724–307, this additional inaccuracy does not substantially increase the error bars on M and R in Table 1.

The determined Eddington flux is smaller than the touchdown flux by about 15%. Half of this difference can easily be explained by the temperature dependence of the electron scattering opacity (Paczynski 1983; Pozdniakov et al. 1983; Lewin et al. 1993). In our model calculations (Suleimanov et al. 2011), we used the Kompaneets equation to describe the electron scattering that assumes the Thomson opacity. Because the upper atmospheric layers can be as hot as 3–3.5 keV, the electron scattering opacity there is smaller than the Thomson opacity by about 6%–8%, and the actual Eddington limit is reached at a correspondingly higher luminosity than L_{Edd} given by Equation (5). Because we fit the data at luminosities much below the Eddington (where the correction to the Thomson opacity is small), we determine F_{Edd} as given by Equation (6), which is used for determining M and R . We also note here that the opacity effect is not included in the touchdown method, which assumes the touchdown flux is equal to the Eddington flux at the Thomson opacity.

The remaining $\sim 8\%$ difference between the “true” Eddington flux and the touchdown flux can be understood if we take into account that the maximum luminosity for PRE bursts can exceed the Eddington luminosity on the surface due to the dependence of the observed Eddington luminosity on the redshift z (see Equation (5) and Lewin et al. 1993). This would imply that the photospheric radius corresponding to the touchdown exceeds the NS radius by $\sim 25\%$. Then, the corresponding color correction has to be $\sim 15\%$ larger than for our models with $l = 0.98$, which is consistent with that expected at $L \sim L_{\text{Edd}}$ (Pavlov et al. 1991). The sharp maximum in T_{bb} (and minimum in K) can arise from a joint influence of the increasing color correction and decreasing effective temperature during the PRE phases.

The lower limit on the NS radius of 13.5–14 km obtained by us is consistent with the measurements for the thermally emitting quiescent NS X7 in the globular cluster 47 Tuc ($14.5^{+1.8}_{-1.6}$ km; Heinke et al. 2006). However, the radii of other thermally emitting quiescent NSs are significantly smaller (9–13 km; Webb & Barret 2007; Guillot et al. 2011). We note that these results depend on the models of the NS hydrogen atmosphere, which were also computed for the passively cooling NSs (Heinke et al. 2006). When a quasi-spherical accretion occurs at a low rate during the quiescence, the additional heat dissipated in the upper atmosphere would increase the temperature there, and, therefore, f_c (see, e.g., Zane et al. 2000). In this case, the NS radius can be underestimated. We also need to note that if the NS in 4U 1724–307 has a spin of 500 Hz, the radius of the non-rotating star would be about 1 km smaller than what is estimated above. Our constraints on the NS radii are in good agreement with the NS radii (13–16 km) evaluated by Suleimanov & Poutanen (2006) from the spectra of low-mass X-ray binaries using the spreading layer model. Rather large NS radii are allowed by the modern equations of state (Hebeler et al. 2010), which predict the upper limit of 13.5 km for a $1.4 M_{\odot}$ NS.

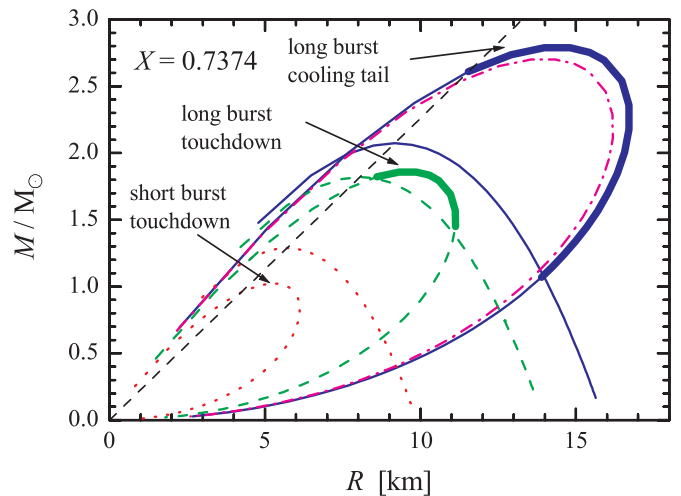


Figure 11. Comparison of the solutions (thick curves) obtained for the long burst using the cooling tail method (solid curves) and the touchdown method (dashed curves), and for the short bursts using the touchdown method only (dotted curves). The curves corresponding to the obtained $T_{\text{Edd},\infty}$ and A (at $D_{10} = 0.47$) are also shown. All solutions are derived for $X = 0.7374$. The dash-dotted curve corresponds to the short burst with $K = 115$, $F_{\text{Edd},-7} = 0.55$, and $f_c = 1.78$ (i.e., $T_{\text{Edd},\infty} = 1.45$ keV).

(A color version of this figure is available in the online journal.)

4.1.2. Touchdown Method

We now apply the touchdown method described in Section 3.3 to the same data on the long burst. This approach is used for illustrative purposes only and here we do not consider any statistical errors. Let us take the Eddington flux equal to the touchdown flux $F_{\text{Edd},-7} = 0.605$, the normalization in the cooling tail $K = 230$, $f_c = 1.4$, and $X = 0.7374$. From these quantities we obtain $T_{\text{Edd},\infty} = 1.84 \times 10^7$ K and an upper limit on the distance $D_{10,\text{max}} = 0.5$. The curves relevant to the derived $T_{\text{Edd},\infty}$ and the distance $D_{10} = 0.47$ (corresponding to a 1σ deviation from the minimal distance of 5.3 kpc) are shown in Figure 11 by dashed lines. Using this approach we can estimate $M \approx (1.6 \pm 0.2) M_{\odot}$ and $R \approx 10.0 \pm 1.5$ km. We see that the touchdown method gives a substantially smaller NS radius compared with the cooling tail method.

The uncertainties in M and R are actually much larger because of the uncertainties in chemical composition, color correction, and distance (see Figure 12). The most significant errors arise due to unknown distance and the hydrogen mass fraction in the NS atmosphere. (See the top panel of Figure 12, where we considered two limiting cases for the distance of $D_{10} = 0.47$ and 0.83 corresponding to 1σ deviations on both ends of the distance distribution and for the hydrogen mass fraction $X = 1$ and 0.) Uncertainties in f_c also affect the results (middle panel of Figure 12), e.g., changing f_c from 1.35 to 1.45 increases the maximum possible R from 10 to 13 km and M from 1.5 to $2 M_{\odot}$. We note that f_c is actually closer to 1.5 for the hydrogen-rich atmospheres (see Figure 6). Less significant errors appear due to uncertainties in the observed Eddington flux on the NS surface (bottom panel of Figure 12). A larger flux corresponds to a smaller M and R .

4.2. Short Bursts

The cooling tracks for the short PRE bursts shown in Figure 9 are very different from that of the long burst and are completely inconsistent with the theoretical dependencies. This is a strong

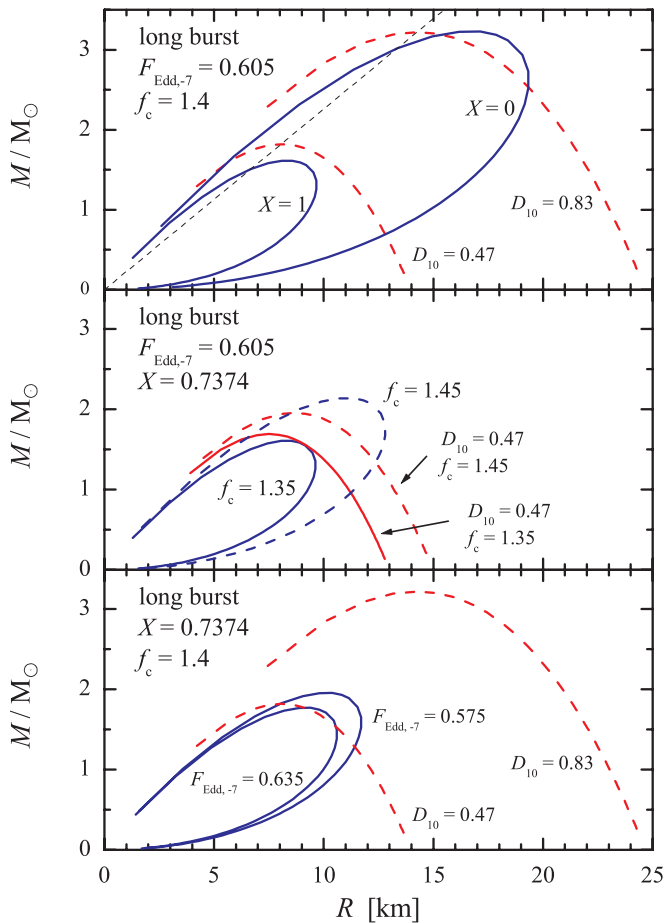


Figure 12. Expected uncertainties for the M and R solutions obtained for the long burst using the touchdown method.

(A color version of this figure is available in the online journal.)

argument that suggests these cooling tracks are affected by some additional physics and cannot be used to determine the NS mass and radius. Ignoring that fact, let us still apply the touchdown method to the short bursts. Taking $F_{\text{Edd},-7} \approx 0.55$ and $K \approx 115$ (see Figure 4) and assuming $f_c = 1.4$, we find that the curves on the M - R plane corresponding separately to constraints from F_{Edd} and K do not cross for hydrogen-rich atmospheres ($X > 0.7374$) at any distance larger than 3.8 kpc, while for $D = 4.7$ kpc they cross only for $X < 0.45$ (see Figures 11 and 9). A situation in which the two observables are consistent with each other in a very restricted range of X and distances is not unique to 4U 1724–307, but it is typical for many bursters, particularly those analyzed by Özel et al. (2009) and Güver et al. (2010a) as shown by Steiner et al. (2010); see Section 5.2 for details. For pure He atmospheres, there are consistent solutions at $M \sim 1.5 M_\odot$ and $R \sim 10$ km at the distance ~ 6 kpc. However, we note again that the results from these short bursts are not reliable because their cooling tracks contradict the theory that the analysis is based on (which predicts $f_c \sim 1.4$ in the cooling tail and much higher at luminosities close to the Eddington).

The measured $K \approx 115$ from the horizontal part of the bottom panel in Figure 4 is two times smaller than the corresponding values for the long burst $K \approx 230$. This can result from two simultaneous effects. The long X-ray burst occurred in the hard state, when the accretion flow in the NS vicinity had a small optical depth that only marginally affects the NS

photosphere and cannot eclipse the NS. On the other hand, the short bursts happened in the soft state, when the persistent emission originated in the optically thick accretion disk and the boundary layer. Therefore, the accretion disk can only block part of the star in the decay phase of the burst, reducing K by a factor of up to two in the case of a large inclination. Even if the inclination is small, the apparent NS area decreases by a factor of $\kappa = 1 - u^2$ (where $u = R_S/R$). These limiting cases can be united in a simple approximate formula for the reduction factor:

$$\kappa = \frac{1}{2}(1 + [1 - 2u^2] \cos i). \quad (21)$$

An additional effect can be related to the optically thick boundary layer. If the spreading layer model describes the boundary layers correctly (Inogamov & Sunyaev 1999), a significant part of the emergent radiation can arise in the rapidly rotating spreading layer above the hot NS surface, which has a reduced effective gravity due to the centrifugal force, resulting in a flux through the atmosphere that is close to the local Eddington limit and has a high color correction $f_c \approx 1.6$ – 1.8 (see Suleimanov & Poutanen 2006) and therefore small K . Using $K^{-1/4} \approx 0.305$ as measured in the short bursts and $A \approx 0.172$ as determined from the long burst, we can then estimate the color correction at the cooling tails of the short bursts $f_c \approx 1.77 \kappa^{1/4}$, which accounts for both effects (see Figure 11). The importance of the spreading layer can vary with the accretion rate, and potentially the normalization values from K for the long burst to $K/2$ can be found (see, e.g., Zhang et al. 2010).

It is also possible that the chemical composition of the NS atmosphere during short and long bursts will be different. For example, pure helium atmospheres give K by 20%–25% larger than pure hydrogen atmospheres because f_c for helium atmospheres is 5%–6% smaller (see Equation (11) and Figure 6). However, the maximum temperature at the touchdown point must be $\approx 20\%$ larger for helium atmospheres (≈ 3.2 keV, see Equation (13)), while the maximum temperatures in the long and short bursts are very close to each other, ≈ 2.7 – 2.8 keV, which argues against a difference in the chemical composition.

5. COMPARISON TO OTHER X-RAY BURSTERS

5.1. Long PRE Bursts

Penninx et al. (1989) analyzed two long-duration (> 100 s) PRE bursts observed by *EXOSAT*/ME in 1984 and 1986 from 4U 1608–52 in its hard state at a rather low persistent flux of $(1\text{--}2) \times 10^{-9}$ erg cm $^{-2}$ s $^{-1}$ in the 2–20 keV band. The evolution of $T_{\text{bb}} F^{-1/4}$ (which is proportional to $K^{-1/4}$) with F , shown in their Figure 7, is almost identical to the models presented in Figure 6 of Suleimanov et al. (2011).

Kuulkers et al. (2003) reported observations by *RXTE*/PCA of the long PRE bursts from 4U 1724–307 (analyzed here), the atoll source 4U 2129+11 in globular cluster M15, and H1825–331 in globular cluster NGC 6652. Spectral evolution after the touchdown in all sources is very similar. Kuulkers et al. (2003) also reported observations by the *BeppoSAX*/Wide Field Camera of 24 long PRE bursts from 4U 1724–307. Spectral evolution during the cooling phases of these bursts is entirely consistent with that observed in the long burst by the *RXTE*/PCA.

Observations by the *Ginga*/Large Area Counter of a long PRE burst from 4U 2129+11 during its island (hard) state at a low persistent flux level of $\sim 0.5 \times 10^{-9}$ erg cm $^{-2}$ s $^{-1}$ are presented by van Paradijs et al. (1990). The behavior of $T_{\text{bb}} F^{-1/4}$

at fluxes above 30% of the peak (touchdown) flux shown in their Figure 10 is very similar to that for the long burst from 4U 1724–307 shown in our Figure 9. For both objects the data at high fluxes are described well by the theory. We note that in both cases the position of the touchdown point in the $K^{-1/4}$ – F diagram is not consistent with the extrapolation of the data from intermediate fluxes, implying that the Eddington flux is smaller than the touchdown flux.

5.2. Short PRE Bursts from EXO 1745–248, 4U 1820–30, and 4U 1608–52

Recently, strong claims have appeared in the literature that suggest that both the NS mass and radius can be determined with an accuracy of better than 10% from the PRE bursts from three NSs: EXO 1745–248 ($M = 1.7 \pm 0.1 M_\odot$, $R = 9 \pm 1$ km; Özel et al. 2009), 4U 1608–52 ($M = 1.74 \pm 0.14 M_\odot$, $R = 9.3 \pm 1.0$ km; Güver et al. 2010a), and 4U 1820–30 ($M = 1.58 \pm 0.06 M_\odot$, $R = 9.1 \pm 0.4$ km; Güver et al. 2010b). The authors of these papers used only short PRE bursts, which, as we have seen above, are suspicious because their spectral evolution is not consistent with the theory that the method is based on. The main reasons for this is probably a partial blocking of the NS by the accretion disk and the effects of the spreading layer on the NS atmosphere. A high declared accuracy cannot be understood in light of all the uncertainties, especially on the distance and the chemical composition (see Figure 12). Below we try to find the answers by critically considering the input numbers and the assumptions made in the aforementioned papers.

5.2.1. EXO 1745–248 in Terzan 5

Özel et al. (2009) have determined the following parameters from the two PRE bursts from EXO 1745–248: $F_{\text{Edd},-7} = 0.625 \pm 0.02$ and $K = 116 \pm 13$. These correspond to $T_{\text{Edd},\infty} = 2.2 \times 10^7$ K and the maximum possible distance (see Equation (20)) $D_{10,\text{max}} = 0.5978$ at $f_c = 1.4$ (which was fixed). For the chemical composition, the authors also assumed pure helium, $X = 0$. The distance was taken to be $D_{10} = 0.63 \pm 0.0315$ (box-car distribution), with the strict lower limit of 0.5985 being very close (within 0.1%) to the maximum possible distance for the observables. As a result, the curves corresponding to $T_{\text{Edd},\infty}$ and K only touch each other (see Figure 13). We note that the assumption of the box-car distribution for the distance (as well as for K) only allows distances within 10% above the used strict lower limit. Thus, Özel et al. (2009) de facto assumed nearly the delta-function distribution of the distance at ~ 6 kpc. Fixing also f_c and X , they also completely removed all uncertainties connected with these parameters. The declared errors in M and R thus reflect the statistical errors in $F_{\text{Edd},-7}$ and K only, which are, of course, small because of the brightness of the considered events. We also note that Ortolani et al. (2007) evaluated the distance to Terzan 5 of 5.5 ± 0.9 kpc and Valenti et al. (2007) gave $D = 5.9$ kpc. Relaxing the assumption of the box-car distribution for the distance (e.g., by using a Gaussian distribution) will inevitably move the solutions toward smaller distances and therefore smaller masses and radii.

5.2.2. 4U 1820–30 in NGC 6624

Using the *RXTE* data for five short PRE bursts from 4U 1820–30, Güver et al. (2010b) determined $F_{\text{Edd},-7} = 0.539 \pm 0.012$ and $K = 92 \pm 2$. These correspond to $T_{\text{Edd},\infty} = 2.25 \times 10^7$ K and the maximum possible distance $D_{10,\text{max}} = 0.617$ at $f_c = 1.4$ and $X = 0$. These authors fixed the chemical composition at $X = 0$ and varied f_c between 1.3 and 1.4 within the

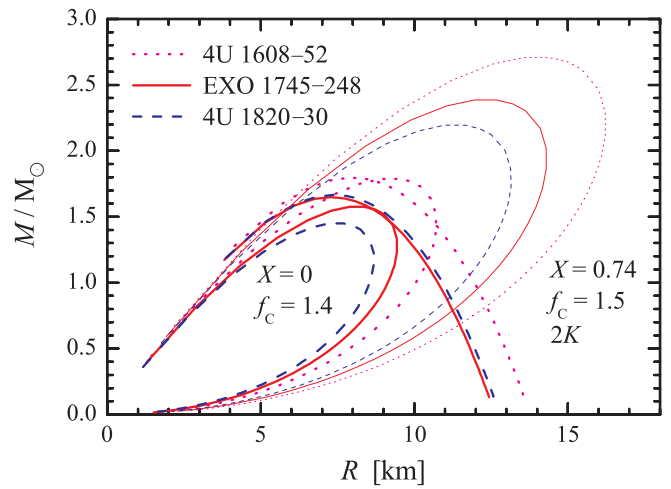


Figure 13. Curves corresponding to constant $T_{\text{Edd},\infty}$ and K (for the strict lower limit on the distance) at $f_c = 1.4$ and $X = 0$ for EXO 1745–248 (thick solid curves), 4U 1820–30 (thick dashed curves), and 4U 1608–52 (thick dotted curves). The contours for constant $T_{\text{Edd},\infty}$ at $f_c = 1.5$ and $X = 0.7374$ for double normalization $2K$ are also presented (thin curves).

(A color version of this figure is available in the online journal.)

strict limits (box-car distribution). Using estimates by Kuulkers et al. (2003) and Valenti et al. (2007), they took the distance to the source $D_{10} = 0.82 \pm 0.14$, but again assumed strict limits (box-car distribution).

Formally, there is no solution possible for these observables because the curves corresponding to $T_{\text{Edd},\infty}$ and K do not cross (see Figure 13). The solutions for the larger distances in the Gaussian tails of the distributions of $F_{\text{Edd},-7}$ and K are still possible with a probability of about 10^{-7} (Steiner et al. 2010). Again, the obtained errors in M and R reflect the statistical errors in $F_{\text{Edd},-7}$ and K only, but the solution is highly unlikely.

As in the case of EXO 1745–248, relaxing the distance constraints to allow smaller distances moves the solution toward smaller distances and smaller M and R . Similar to the case of the short bursts from 4U 1724–307, the spectral evolution of the considered bursts is not consistent with the theory. The value of $K^{-1/4}$ drops by only 12% after the touchdown, while the theory predicts a 20% variation.

5.2.3. 4U 1608–52

Using the data from four PRE bursts and one non-PRE burst from 4U 1608–52, Güver et al. (2010a) found the following observables: $F_{\text{Edd},-7} = 1.541 \pm 0.065$ and $K = 324.6 \pm 2.4$. These correspond to $T_{\text{Edd},\infty} = 2.13 \times 10^7$ K and the maximum possible distance $D_{10,\text{max}} = 0.405$ at $f_c = 1.4$ and $X = 0$. The chemical composition was allowed to vary from $X = 0$ to 0.7, and f_c within the interval between 1.3 and 1.4 with the strict limits. The distance was taken by these authors as $D_{10} = 0.58^{+0.2}_{-0.18}$, with the strict lower limit being equal to 3.9 kpc. In this case, this lower limit is smaller than the maximum possible distance, so the solutions exist (the curves corresponding to $T_{\text{Edd},\infty}$ and K do cross; see Figure 13). Formally, the authors allow a wide range of variation for X , but, in reality, only solutions with $X \leq 0.04$ are possible. At a larger X , the maximum possible distance becomes smaller than the strict lower limit on the distance of 3.9 kpc. As in the previous two cases, relaxing the distance constraints to allow for smaller distances will move the solution toward smaller distances and smaller M and R .

We also note here that bursts selected by Güver et al. (2010a) occurred at a high accretion rate in the soft state. The normalization K is nearly constant during the cooling tails, which strongly contradicts the theory. On the other hand, the PRE bursts happening at a low accretion rate follow the spectral evolution predicted by the theory, have normalization K about 60% larger, and, of course, the NS mass and radius determined from these data are also different (J. Poutanen et al. 2011, in preparation).

5.2.4. Summary

We conclude that small uncertainties in M and R obtained for the three bursters are the direct consequence of fixing the color correction f_c , hydrogen mass fraction X , and, most importantly, the assumed strict lower limit in the distance distribution, which only allows solutions at its lower edge. The lower limits on the distance assumed by the authors in two cases turned out to be very close to the maximum possible distance allowed by the observables. This completely removed all of the uncertainties in the distance. Assuming a Gaussian distribution in distance allows solutions with much smaller (probably unphysical) M and R for all three sources.

The results of the spectral fitting for the short PRE bursts for these three NSs are very close to the results obtained for the short bursts of 4U 1724–307. We suggest that during short bursts roughly one-half of the NS is visible, most probably due to the eclipse by the accretion disk. Taking the apparent area to be twice that of the observed one, the determined NS radii move to the values consistent with those determined from the long burst from 4U 1724–307 (see Figure 13). Additional corrections are also possibly needed because of the influence of the boundary layer on the dynamics and the spectral properties of the bursting atmosphere, resulting in a higher color correction $f_c \sim 1.6$ –1.8.

Recently, Steiner et al. (2010) have suggested that the absence of the solutions for short bursts mentioned above can be fixed by relaxing the assumption that the Eddington flux is reached at the moment of touchdown (or, rather, that the photosphere at touchdown is not at the NS surface). This, however, does not solve the problem because the determined blackbody normalization in the cooling tail and the Eddington flux is not reliable in these short PRE bursts and the assumed distance constraints were too strict. Because the spectral evolution during the cooling tails of the short PRE bursts (at high persistent luminosity) strongly contradicts the theory, the results obtained from these data are questionable. To determine the NS masses and radii we suggest only using those data that do follow the theory.

6. CONCLUSIONS

We applied a recently computed, detailed set of NS atmosphere models covering a large range of luminosities (Suleimanov et al. 2011) to the data of the PRE bursts of 4U 1724–307. We showed that the variation of the apparent blackbody radius during the cooling stage of the 150 s long PRE X-ray bursts in 4U 1724–307 is entirely consistent with the theoretical color-correction–flux dependence at intermediate fluxes. We thus obtained the Eddington flux and the apparent NS radius (divided by the distance to the source). We found that the Eddington flux (for the Thomson opacity) is not reached at the so-called touchdown point but rather at a 15% lower luminosity. We constrained the mass and radius of the NS using the estimated distance to the source. We found a lower limit on the stellar radius of ~ 14 km for $M < 2.3 M_\odot$ at a 90%

confidence level independently of chemical composition. (If the NS in 4U 1724–307 has a spin of 500 Hz, the radius of the non-rotating star would be about 1 km smaller.) Smaller radii are possible only for a more massive NS. These results support a stiff equation of state for the NS matter. We showed that hydrogen-rich accreting matter is preferred, and we obtained an upper limit on the distance to 4U 1724–307 of about 7 kpc.

We have also demonstrated that the cooling tracks of the short PRE bursts from 4U 1724–307 that occurred during the high/soft state do not follow the evolution expected from the theory, and the NS apparent areas are a factor of two smaller than that for the long burst. The probable reason for this is the partial eclipse of the NS surface by the optically thick accretion disk. An additional spectral hardening during the cooling tails associated with the influence of the boundary/spreading layer can also be important. Therefore, the constraints on the NS mass and radius obtained from such bursts are not reliable.

Finally, we showed that previous analyses of the short PRE bursts from three sources, EXO 1745–248, 4U 1820–30, and 4U 1608–52, are questionable because they ignore the fact that spectral evolution during the bursts is not consistent with the theory for the passively cooling unobscured NS, which is the basis for the analysis. Assuming that the touchdown flux is reached when the photosphere is detached from the NS surface (Steiner et al. 2010) does not solve the problem because the determined blackbody normalization in the cooling tail and the Eddington flux are not reliable in these short bursts.

We suggest that only PRE bursts showing spectral evolution consistent with the theory should be used when estimating NS masses and radii. Further improvement in the accuracy of the determination of the NS parameters requires new atmosphere models with the exact Compton scattering kernel, as well as accounting for the Doppler effect due to the rapid NS rotation. Rotation also introduces additional distortion to the NS spectra because of the difference in the effective gravity at the stellar poles and the equator due to the centrifugal force. We plan to investigate the importance of these effects in future work.

The work is supported by the German Research Foundation (DFG) grant SFB/Transregio 7 “Gravitational Wave Astronomy” (V.S., K.W.), Russian Foundation for Basic Research (grant 09-02-97013-r-povolzhe-a, V.S.), the Academy of Finland (grant 127512, J.P.), and DFG cluster of excellence “Origin and Structure of the Universe” (M.R.). We thank Dmitry Yakovlev for a number of useful suggestions.

REFERENCES

- Arnaud, K. A. 1996, in ASP Conf. Ser. 101, *Astronomical Data Analysis Software and Systems V*, ed. G. H. Jacoby & J. Barnes (San Francisco, CA: ASP), 17
- Damen, E., Magnier, E., Lewin, W. H. G., et al. 1990, *A&A*, **237**, 103
- Ebisuzaki, T. 1987, *PASJ*, **39**, 287
- Galloway, D. K., Munro, M. P., Hartman, J. M., Psaltis, D., & Chakrabarty, D. 2008a, *ApJS*, **179**, 360
- Galloway, D. K., Özel, F., & Psaltis, D. 2008b, *MNRAS*, **387**, 268
- Grebel, E. K., & Roberts, W. J. 1995, *A&AS*, **109**, 293
- Guillot, S., Rutledge, R. E., & Brown, E. F. 2011, *ApJ*, **732**, 88
- Güver, T., Özel, F., Cabrera-Lavers, A., & Wroblewski, P. 2010a, *ApJ*, **712**, 964
- Güver, T., Wroblewski, P., Camarota, L., & Özel, F. 2010b, *ApJ*, **719**, 1807
- Haensel, P., Potekhin, A. Y., & Yakovlev, D. G. 2007, *Neutron Stars 1: Equation of State and Structure* (Astrophysics and Space Science Library, Vol. 326; New York: Springer)
- Hebeler, K., Lattimer, J. M., Pethick, C. J., & Schwenk, A. 2010, *Phys. Rev. Lett.*, **105**, 161102

- Heinke, C. O., Rybicki, G. B., Narayan, R., & Grindlay, J. E. 2006, [ApJ](#), **644**, 1090
- Inogamov, N. A., & Sunyaev, R. A. 1999, *Astron. Lett.*, **25**, 269
- Jahoda, K., Markwardt, C. B., Radeva, Y., et al. 2006, [ApJS](#), **163**, 401
- Kirsch, M. G., Briel, U. G., Burrows, D., et al. 2005, [Proc. SPIE](#), **5898**, 22
- Kuchinski, L. E., Frogel, J. A., Terndrup, D. M., & Persson, S. E. 1995, [AJ](#), **109**, 1131
- Kuulkers, E., den Hartog, P. R., in't Zand, J. J. M., et al. 2003, [A&A](#), **399**, 663
- Lattimer, J. M., & Prakash, M. 2007, [Phys. Rep.](#), **442**, 109
- Lewin, W. H. G., van Paradijs, J., & Taam, R. E. 1993, [Space Sci. Rev.](#), **62**, 223
- London, R. A., Howard, W. M., & Taam, R. E. 1984, [ApJ](#), **287**, L27
- London, R. A., Taam, R. E., & Howard, W. M. 1986, [ApJ](#), **306**, 170
- Madej, J. 1991, [ApJ](#), **376**, 161
- Madej, J., Joss, P. C., & Róžańska, A. 2004, [ApJ](#), **602**, 904
- Majczyna, A., Madej, J., Joss, P. C., & Róžańska, A. 2005, [A&A](#), **430**, 643
- Molkov, S. V., Grebenev, S. A., & Lutovinov, A. A. 2000, [A&A](#), **357**, L41
- Ortolani, S., Barbuy, B., Bica, E., Zoccali, M., & Renzini, A. 2007, [A&A](#), **470**, 1043
- Ortolani, S., Bica, E., & Barbuy, B. 1997, [A&A](#), **326**, 614
- Özel, F., Güver, T., & Psaltis, D. 2009, [ApJ](#), **693**, 1775
- Paczynski, B. 1983, [ApJ](#), **267**, 315
- Pavlov, G. G., Shibano, I. A., & Zavlin, V. E. 1991, *MNRAS*, **253**, 193
- Penninx, W., Damen, E., van Paradijs, J., Tan, J., & Lewin, W. H. G. 1989, [A&A](#), **208**, 146
- Pozdniakov, L. A., Sobol, I. M., & Sunyaev, R. A. 1983, *Astrophys. Space Phys. Rev.*, **2**, 189
- Rutledge, R. E., Bildsten, L., Brown, E. F., Pavlov, G. G., & Zavlin, V. E. 2002, [ApJ](#), **577**, 346
- Steiner, A. W., Lattimer, J. M., & Brown, E. F. 2010, [ApJ](#), **722**, 33
- Strohmayer, T., & Bildsten, L. 2006, in *Cambridge Astrophysics Series 39, Compact Stellar X-Ray Sources*, ed. W. Lewin & M. van der Klis (Cambridge: Cambridge Univ. Press), 113
- Suleimanov, V., Madej, J., Drake, J. J., Rauch, T., & Werner, K. 2006, [A&A](#), **455**, 679
- Suleimanov, V., & Poutanen, J. 2006, [MNRAS](#), **369**, 2036
- Suleimanov, V., Poutanen, J., & Werner, K. 2011, [A&A](#), **527**, A139
- Suleimanov, V., & Werner, K. 2007, [A&A](#), **466**, 661
- Valenti, E., Ferraro, F. R., & Origlia, L. 2007, [AJ](#), **133**, 1287
- van Paradijs, J., Dotani, T., Tanaka, Y., & Tsuru, T. 1990, *PASJ*, **42**, 633
- Webb, N. A., & Barret, D. 2007, [ApJ](#), **671**, 727
- Weisskopf, M. C., Guainazzi, M., Jahoda, K., et al. 2010, [ApJ](#), **713**, 912
- Zane, S., Turolla, R., & Treves, A. 2000, [ApJ](#), **537**, 387
- Zavlin, V. E., Pavlov, G. G., & Shibano, Y. A. 1996, [A&A](#), **315**, 141
- Zhang, G., Mendez, M., & Altamirano, D. 2010, [MNRAS](#), **413**, 1913